Effects of clamp rise-time on rat brain IIA sodium channels in *Xenopus* oocytes

Peter C. Ruben [a,*], Andrea Fleig [1,c], David Featherstone [a], John G. Starkus [b],
Martin D. Rayner [c]

[a] *Department of Biology, Utah State University, Logan, Utah 84322-5305, USA*
[b] *Békésy Laboratory of Neurobiology, Pacific Biomedical Research Center, University of Hawaii at Manoa, Manoa, USA*
[c] *Department of Physiology, John A. Burns School of Medicine, University of Hawaii at Manoa, Manoa, USA*

Abstract

The kinetic properties of wild-type rat brain IIa sodium channels in excised macropatches were studied using step depolarizations and ramp depolarizations to imitate the slow settling-time of voltage in two-electrode voltage clamp. Ramp depolarizations longer than 1 ms produce an increasing suppression of peak sodium current (I_{Na}). Two rates of inactivation can be seen in macroscopic sodium current records from excised patches following both step and ramp depolarizations. During slow ramp depolarizations, reduction in peak I_{Na} is associated with selective loss of the fastest rate of test-pulse inactivation. This change can be interpreted as resulting from inactivation of a separate sub-population of 'fast mode' channels. The slow rate of test-pulse inactivation is relatively unaffected by changing ramp durations. These results are sufficient to explain the typically slow inactivation kinetics seen in two-electrode voltage clamp recordings of sodium channels in *Xenopus* oocytes. Thus, the kinetics of sodium channels expressed in *Xenopus* oocytes are not readily characterizable by two-electrode clamp because of the large membrane capacitance and resulting slow clamp settling time which artifactually selects for slow mode channels. © 1997 Elsevier Science B.V.

Keywords: Sodium channel; Oocyte; Patch clamp; Two electrode voltage clamp

1. Introduction

Voltage-gated sodium channels mediate the very rapid rising phase and initial component of the falling phase of action potentials in many excitable cells (Hodgkin and Huxley, 1952; Hille, 1992). The channel protein undergoes extremely fast changes in conformation which lead to pore opening (activation) (Stühmer et al., 1989) and blocking (fast inactivation) by an intracellular component of the molecule (Patton et al.,

1992; West et al., 1992). In central nervous system neurons, the peak of the action potential is reached in < 0.5 ms (Lux and Pollen, 1966; McCormick et al., 1985). Fast inactivation has been observed to proceed with at least two distinct rates (fast and slow components or 'modes') in both native channels (Chiu, 1977; Patlak and Ortiz, 1985, 1986; Huguenard et al., 1988; Cummins et al., 1994) and in channels expressed in heterologus systems (Zhou et al., 1991; Fleig et al., 1994a).

mRNA coding for the a subunit of rat brain sodium channels is sufficient to form functional channels (Goldin et al., 1986). However, when expressed in *Xenopus* oocytes and studied with two-electrode voltage clamp (TEV), these channels have been reported to show abnormally slow rates of activation and, particu-

* Corresponding author. Tel.: + 1 801 7972490; fax: + 1 801 7971575; e-mail: pruben@cc.usu.edu
[1] Present Address: Department of Membrane Biophysics, Max Planck Institute for Biophysical Chemistry, Am Fassberg, D-37077 Göttingen, Germany.

larly, test-pulse inactivation (Auld et al., 1988; Krafte et al., 1990). For this reason, other expression systems (Li et al., 1992) and/or co-expression of the $\beta 1$ subunit in oocytes (Isom et al., 1992; McClatchey et al., 1993; Yang et al., 1993) have been cited as necessary to record activation and inactivation kinetics that resemble those of native sodium channels. On the other hand, relatively little has been noted about the properties inherent to different recording techniques and how these might affect sodium current waveforms. Whereas patch clamp techniques have been used for recording sodium currents in Chinese hamster ovary cells (Scheuer et al., 1990) and human embryonic kidney cells (Ukomadu et al., 1992; Cummins et al., 1993), a majority of the studies of channels in oocytes use the convenient two-electrode voltage clamp method. This method is particularly well-suited to oocyte work because of the cells' large diameter. However, the very property that makes these cells easy to study produces a large cell capacitance which necessarily slows clamp rise time. Effects of clamp rise time in artifactual 'elimination' of fast transients have been presented for IgON (Alicata et al., 1989). We here demonstrate that a similar effect, using much slower clamp rise times, 'eliminates' the fast component of I_{Na}.

We have studied macroscopic currents from rat brain IIa (RBIIa) sodium channel a subunits expressed in *Xenopus* oocytes using both two-electrode voltage clamp and excised inside-out macro-patches. We here compare the results of studies using these two methods, and demonstrate that fast rates of both activation and inactivation, resembling native channels, can be recorded from excised macropatches (patch clamp). By contrast, we show that slow kinetics similar to those recorded in two-electrode voltage clamp can be mimicked in patch clamp by using slow depolarizing voltage ramps, instead of 'instantaneous' voltage steps, which 'eliminate' the fast component of I_{Na} similar to the effect of slow clamp rise time on IgON (Alicata et al., 1989). These results have been previously presented in abstract form (Ruben et al., 1993).

2. Methods

Stage V-VI oocytes were taken from adult female *Xenopus laevis* and isolated using 2 mg/ml collagenase (Sigma or Boehringer-Mannheim) in Ca^{++}-free Ringer containing (in mM): 82.5 NaCl, 2 KCl, 1 $MgCl_2$, 5 HEPES at pH 7.5 for 45–90 min. The oocytes were subsequently rinsed and maintained in Ca^{++}-free Ringer before and during mRNA injection.

Sodium channel cDNA was obtained as previously described (Fleig et al., 1994b). mRNA for injection was made from template rat brain IIa cDNA using an in vitro transcription kit (Promega or Ambion). Ten to 50

ng of mRNA thus produced was injected into oocytes, 2–3 h after isolation, using an automatic injector (Drummond Scientific). After mRNA injection, oocytes were transferred to a standard Ringer solution (ND96) with (in mM) 96 NaCl, 4 KCl, 1.8 $CaCl_2$, 1 $MgCl_2$, 5 HEPES, pH 7.4 at 18°C.

Three to 10 days after mRNA injection, oocytes were tested for sodium channel expression using two electrode voltage clamp (Warner Instruments). Electrodes were fabricated from thin-walled borosilicate glass (World Precision Instruments) on a horizontal puller (Sutter) with resistances of 0.7 MΩ (current electrode) and 1.5 MΩ (voltage electrode) when filled with 3 M KCl. Measurements were made from oocytes in a bath solution of Ca^{++}-free Ringer (see above) to prevent Ca^{++} influx into the oocytes. Holding potential (V_{hold}) was -120 mV. Data were collected and analyzed using pCLAMP software (Axon Instruments).

Oocytes with at least 2 μA of whole-cell current, as assayed by two electrode voltage clamp, were used for macro-patch recording. Vitelline membranes were manually removed while exposing the oocyte to a hyperosmotic medium containing ND96 with 200 mM K-glutamate added (400 mOsm). Oocytes were transferred to a chamber containing (in mM) 9.6 NaCl, 88 KCl, 1 $CaCl_2$, 1 $MgCl_2$, 11 EGTA, 5 HEPES at pH 7.4. Patch pipets were made from aluminosilicate glass (Sutter or World Precision Instruments) and pulled to resistances of 0.7–1.5 MΩ when filled with ND96. After giga-ohm seals were obtained, patches were excised into the inside-out conformation and maintained at a V_{hold} of -100 mV. Prior to each test pulse, membrane potential was stepped to either -120 or -150 mV for 200 ms to remove fast inactivation. Patch data were acquired using an EPC-9 amplifier controlled by an ITC-16 interface (Instrutech) and a Macintosh Quadra 700 computer running HEKA Pulse and Pulsefit software. Initial data analysis was performed using Pulsefit. Subsequent analysis and curve fitting were done using TempleGraph (Mihalisin Association) running on a Sparc workstation (Sun Microsystems, Mountain View, CA). Some data traces were digitally filtered using an in-house program. All experiments were performed at room temperature (22°C).

2.1. Measurement of clamp rise-time

Where linear capacity currents are dominated by membrane capacitance, clamp rise time can be determined by integration of the capacity transients and measuring the time at which the integration reaches a plateau (Alicata et al., 1989). This situation is approximated when a metal shielding plate is used to reduce stray capacitance between the two electrodes in TEV recording. We have therefore used this method to determine the clamp rise-time in our two-electrode voltage

clamp. However, membrane capacitance is a minimal component of macropatch capacity transients where stray capacitance from even coated glass patch pipets contributes the greatest proportion of the linear capacitance. Integration of the capacity transient in this case gives a spuriously long estimate of clamp rise-time. In this case, we used the rate of current relaxation during small voltage steps between positive test potentials where no significant deactivation occurs. Under these conditions change in driving force fully controls the current relaxation, directly indicating the clamp speed.

2.2. Computer simulations

Simulations were carried out on a Sun SPARCstation LX. Our modeling program uses simple Euler integration to solve the array of simultaneous equations representing the allowed transitions for each model run. For the simple Eyring rate models used here, where all transitions were presumed to have some voltage sensitivity, and where K_α represents the rate constant for the forward (depolarization-favored) reaction and K_β is the back reaction rate, then:

$$K_\alpha = A* \exp^{([ezd(V_m - V_{0.5})]/kT)} \qquad (1)$$

$$K_\beta = A* \exp^{([-ez(1-d)(V_m - V_{0.5})]/kT)} \qquad (2)$$

where e is the electronic charge, z is the valence, d is the barrier position expressed as a fraction of the distance along the reaction coordinate from the depolarization-favored well, V_m is the membrane potential, $V_{0.5}$ is the midpoint voltage, A is the rate constant when $V_m = V_{0.5}$, k is the Boltzmann constant and T is the absolute temperature. See Table 3 for simulation parameters.

Voltage clamp steps with non-instantaneous rise times were simulated as follows; first, state occupancies at holding potential were calculated as the end occupancy following a 500 ms pulse to holding potential. Second, the simulated voltage clamp rise time was provided as an input to the model program. Thereafter, reaction rates were recalculated at 1-μs intervals until the simulated clamp reached command potential. All integrations were carried out using an internal loop time of 0.1 μs. Peak current for the 100 μs exponential clamp rise time (used here for simulation of control voltage steps in macropatch recording) was identical to the peak current for an instantaneous voltage step, although both time to peak and the greater part of the rising phase were right-shifted by about 100 μs.
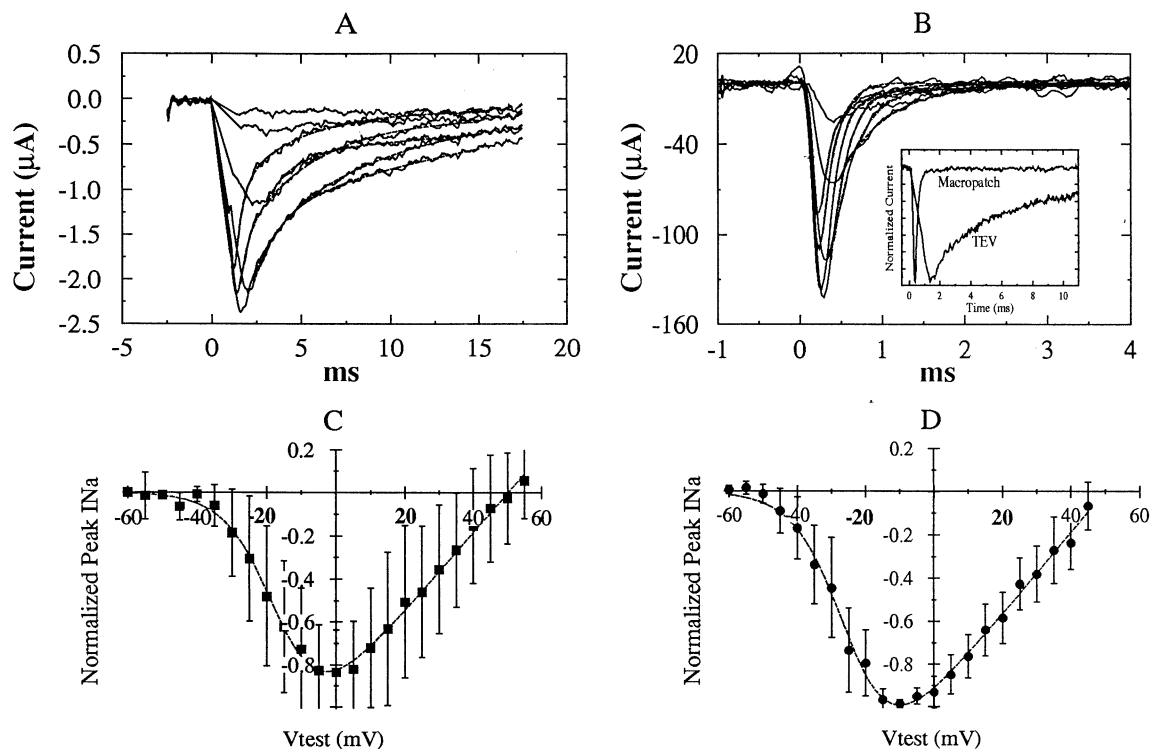

Fig. 1. Comparison of current waveforms and I(V) relationships between TEV and macropatch. (A) Sodium currents recorded with TEV. $V_{hold} = -120$ mV, $V_{test} = -40$ to $+20$ mV in steps of 10 mV. (B) Sodium currents recorded from excised, inside-out macropatch; 200 ms $V_{pre} = -120$ mV, $V_{test} = -40$ to $+20$ mV in steps of 10 mV. Dashed lines show two-exponential fits to the current records. See Table 1 for fit parameters. Note different time scales for A and B. Inset shows I_{Na} waveforms recorded using TEV and macropatch directly compared on the same time scale. Records were normalized to align peak current amplitudes. V_{hold} and $V_{pre} = -120$ mV. $V_{test} = 0$ mV. (C) Mean $\pm$ S.D., $N = 16$ I(V) relationship for I_{Na} recorded with TEV. $V_{hold} = -120$ mV. (D) Mean $\pm$ S.D., $N = 13$) I(V) relationship for I_{Na} recorded with macropatch. $V_{pre} = -120$ mV. See text and Table 2 for I(V) fit parameters.

3. Results

Fig. 1A shows a typical TEV recording from *Xenopus* oocytes expressing the α-subunit of RBIIa sodium channels. Current has been leak-subtracted using a p/4 protocol. This pulse protocol effectively removes linear capacity currents, even where direct observation of the capacity transient (prior to subtraction) indicates that peak I_{Na} was reached before the clamp had settled to command potential. We find that TEV capacity transients last longer than 2 ms in the worst case and around 500 μs in the best case.

For comparison, Fig. 1B shows a family of sodium currents recorded at different command potentials from an excised, inside-out macropatch. In this case, the voltage settles in 40 μs to 150 μs. In both the TEV and macropatch records, test-pulse (fast) inactivation was best fit by a double exponential waveform using Eq. (3):

$$y = (I_{h1}*\exp^{-x/\tau_{h1}}) + (I_{h2}*\exp^{-x/\tau_{h2}}) + b \qquad (3)$$

where I is the intercept at peak current and τ is the time constant for the first (h1) and second (h2) inactivation components, and b is the background, steady-state current at the end of the pulse. Fits to the current records are shown as dashed lines. The results of the fitting protocol for fast inactivation at 0 mV test potential are shown in Table 1 for a typical TEV experiment and a typical macropatch experiment. Note the similarity between τ_{h1} in TEV and τ_{h2} in the macropatch step. The inset in Fig. 1B compares a TEV record with a macropatch record on the same time scale. Both records were obtained by step depolarizations from -120 mV to 0 mV.

Fig. 1C shows mean I(V) relationships ($N = 16 \pm$ S.D.), derived from a series of step depolarizations from a holding potential of -120 mV in TEV. These data were fit with a Boltzmann function of the form shown in Eq. (4):

$$I_{Na} = (V_m - E_{Na})*(g_{Max}/[1 + \exp^{-z(V_m - V_{0.5})/kT}]) \qquad (4)$$

where V_m is the test potential, $V_{0.5}$ is the midpoint voltage, E_{Na} is the observed (extrapolated or interpolated) reversal potential, z is the valence and g_{max} is the maximum conductance, k is the Boltzmann constant and T is absolute temperature. The fit parameters for

the data in Fig. 1D are shown in Table 2. In Fig. 1D, mean I(V) data ($N = 13 \pm$ S.D.) from macropatch recordings are plotted and fit by a line using Eq. (4). The fit parameters for these mean data are also shown in Table 2.

Slow settling time of the TEV does not alone seem sufficient to explain the differences in inactivation time constants seen in Fig. 1 and Table 1. We therefore explored the effects of slow settling time by a direct experimental approach.

To record macroscopic currents without artifacts caused by large membrane surface area, we used macro-patch techniques on oocytes expressing at least 2 μA of current (when assayed using TEV). Since it is difficult (using commercially-available data acquisition software) to duplicate the exponential waveform by which the TEV reaches command potential, we instead used ramp depolarizations of differing durations to study the effects of non-'instantaneous' voltage changes on sodium channel activation and inactivation kinetics. Fig. 2A compares the response of RBIIa sodium channels, recorded in excised, inside-out macropatches, to both 'instantaneous' and ramp depolarizations. The first (left-most) current trace was produced by a step depolarization from -150 mV to a test potential of 0 mV. The next five traces were produced by ramp depolarizations from the same holding potential to the same test potential in response to ramps of 1, 2, 3, 4, and 5 ms durations. Peak current amplitude is reduced and the time to peak current is delayed when ramps rather than step depolarizations are used to generate sodium currents. In the currents produced by >1 ms ramps, peak current is reached before the final test potential is attained. This observation is demonstrated in Fig. 2B, where the time to peak current has been plotted as a function of ramp duration. Times to peak were divided by the ramp duration to generate y-values such that, where time to peak is less than the ramp duration, the y-value would be less than 1.

The decline in peak sodium current amplitude as a function of ramp duration is shown in Fig. 3A. Currents were normalized to the peak current amplitude evoked by a step depolarization to the test potential of 0 mV. The decrease in peak amplitude could be due to a uniform loss of channels by inactivation. However, we have previously demonstrated the presence of two kinetic modes in sodium channels (Fleig et al., 1994a,b),

Table 2
I(V) Fit parameters

Recording method	Slope factor (z)	$V_{1/2}$ (mV)	E_{Na} (mV)	g_{max}
TEV	3.4 e	-15	50	0.018
Macro-patch	3.3 e	-24	50	0.019

Table 1
Inactivation parameters at 0 mV

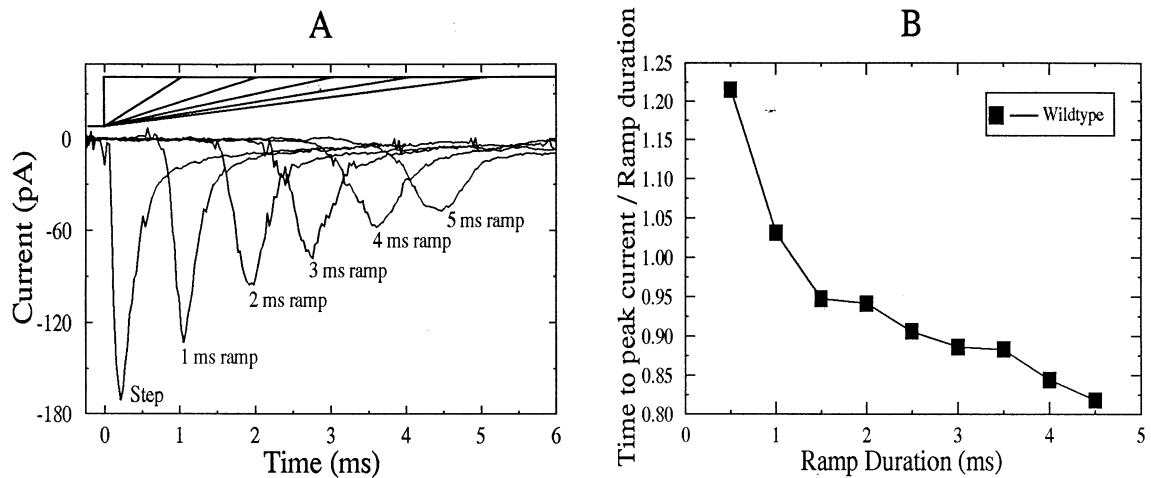| Recording method	I_{h1}	τ_{h1}	I_{h2}	τ_{h2}
TEV	-0.55 μA	1.14 ms	-1.56 μA	7.01 ms
Macropatch step	-133.6 pA	0.17 ms	-4.4 pA	1.12 ms
Macropatch ramp (2 ms)	-56.2 pA	0.29 ms	-14.2 pA	2.56 ms

Fig. 2. (A) RBIIa sodium currents (lower traces) in response to step and ramp depolarizations (upper traces). (B) Macro-patch recordings of sodium channels show that, as ramp duration increases from 0.5 to 4.5 ms, time to peak current increases. However, peak current is reached prior to final test potential in ramps greater than 1 ms in duration. V_{hold} was -100 mV. V_{test} was 0 mV.

indicated by the two components of test-pulse inactivation, as seen in the macroscopic current records of Figs. 1 and 2 (see also Table 2). An alternative explanation for the loss of peak current could be that one kinetic mode is more sensitive to ramp depolarizations. The data in Fig. 3A were best fit by a single exponential, suggesting a uni-modal loss of sodium channels as ramp duration increases from 0.5 to 5.5 ms. To test this idea, we fit double exponentials (see Eq. (3)) to the inactivation phase of currents elicited by step and ramp depolarizations. Although the time constants (τ_{h1} and τ_{h2}) did not significantly change, the intercept of the fast component decreased when ramp durations were longer than about 1 ms, and decayed to 50% in 3–4 ms. By contrast, the intercept of the slow component decayed much more slowly, with no significant decrease until ramp durations of about 5.5 ms were reached. These data are shown in Fig. 3B. Thus, the loss of peak I_{Na} is primarily associated with the concurrent loss of the fast component of test-pulse inactivation.

Although inactivation is usually dominated by the fast rate, some patches only exhibit predominantly slow inactivation kinetics. To further test the hypothesis that sensitivity to ramp depolarizations is primarily due to loss of the fast-mode channels through inactivation, we studied ramp sensitivity in slow-mode patches (where the intercept of the slow rate of test-pulse inactivation was at least 70% of the peak current). Fig. 4A shows currents recorded in a slow-mode patch in response to step and ramp depolarizations. Although there is as slight decrement in the peak current amplitude with increasing ramp durations, the effect is not as pronounced as in fast-mode patches (compare Fig. 4A with Fig. 2A). The relationship between peak current and ramp duration for slow-mode patches is graphed in Fig. 4B (solid boxes) which shows that there was little

decrease in current amplitude with increasing ramp durations (compare with Fig. 2AFig. 3A). These slow-mode current records were best fit with a single exponential using Eq. (5) below:

$$y = (I_{h1} * \exp^{-x/\tau_{h1}}) + b \tag{5}$$

and Fig. 4B shows that the intercepts at peak (open circles) of slow-mode inactivation were not affected by increasing the duration of ramp depolarizations. Time constants ($\tau_h \cong 5$ ms) were similarly unaffected.

4. Discussion

We have shown the following: (1) sodium currents recorded with TEV appear to have slower inactivation kinetics than when recorded in excised macropatches; (2) the apparent slowing by TEV (relative to macropatch) can be mimicked by using 1.5–5.5 ms ramps to depolarize channels in excised macropatches; (3) the apparent slowing during ramp depolarization is due to the progressive loss of a fast component of test-pulse inactivation. This component also appears relatively suppressed in TEV. Thus, TEV (and slow ramp depolarizations in macropatch) select for slowly inactivating channels shown by decreasing fast component intercept (but not rate) during progressively longer ramp depolarizations, whereas the slow component intercept and rate remain unaffected. We conclude that the fast component of test-pulse inactivation is inactivated during the slow rise to test potential in TEV and during macropatch ramp depolarizations. This can be seen from the typical data in Table 1, where the fastest inactivation rate (τ_{h1}) in TEV nearly matches the slowest rate (τ_{h2}) recorded in the cell-free macropatch. Although the removal of cytosolic factors could account
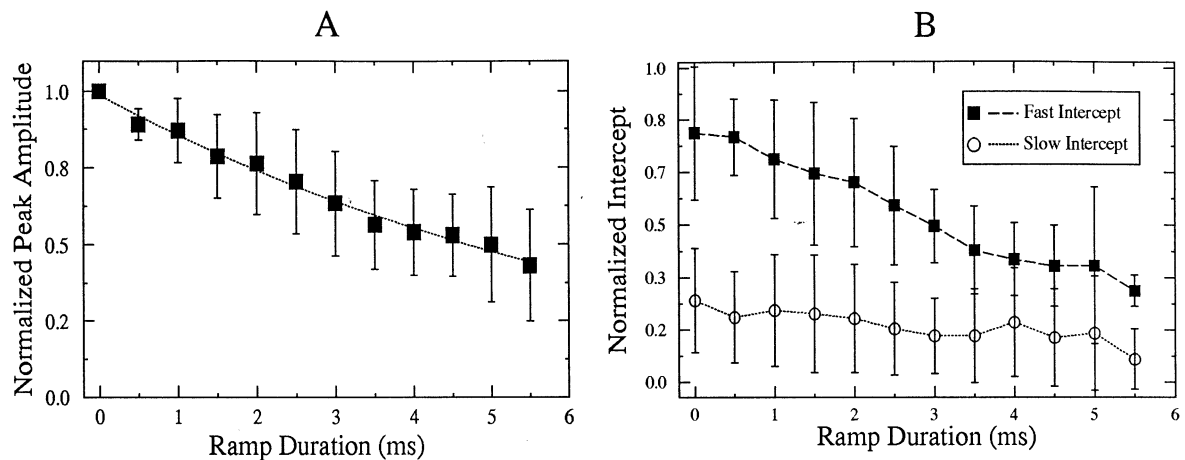
Fig. 3. Sensitivity of peak I_{Na} and intercepts of τ_{h1} and τ_{h2} to ramp duration. (A) Shows the loss of peak sodium current during ramp depolarizations. Current amplitudes were normalized to the peak of the current evoked by a step depolarization (ramp duration = 0). (3) Data were obtained by double exponential fitting to the inactivation phase of currents from step (ramp duration = 0) and ramp depolarizations. Fast and slow component intercepts (I_{h1} and I_{h2} in Eq. (3)) were measured by extrapolation to the time of peak current, and normalized to the maximum value for I_{h1}. Mean values shown ($\pm$ S.D.; $N = 7$ patches). $V_{pre} = -120$ mV. $V_{test} = 0$ mV.

for the differences observed between TEV and excised inside-out patches, cell-attached patches show identical kinetics to excised patches (data not shown). It is therefore unlikely that the differences can be accounted for by the absence of cytosolic control factors in inside-out patches. Another cause underlying the differences could be a lack of spatial homogeniety of membrane voltage (Kass et al., 1979; Schreibmayer et al., 1994). Such conditions, which result in poor space clamp could potentially be compensated through the use of multiple current-injecting electrodes to promote more uniform membrane voltage. We have explored spatial non-uniformities of voltage in oocytes using multiple electrodes and multiple penetrations, and have found the problem to be substantial.

Our results indicate that significant time and voltage artifacts are introduced by slow clamp rise time, such as is often the case in TEV. These problems are illustrated in Fig. 5 where we compare the time course of sodium currents, recorded in a macropatch, with a typical capacity transient recorded with TEV. We have previously established the validity of integrating capacity current to determine clamp rise-time where the capacity transient is predominantly due to membrane capacitance (Alicata et al., 1989). In Fig. 5, we integrated the TEV capacity current from an 80 mV depolarization. Voltage reaches 95% of V_{test} in approximately 0.75 ms. By contrast, the peak of sodium current at -20 mV is reached in about 0.3 ms at which time voltage has only attained approximately 77% of its final value. At 0 mV, peak macropatch current is reached in about 0.25 ms where the TEV voltage is at about 63% of V_{test}. Time to peak is slower with smaller depolarizations. At V_{test} -40 mV, macropatch current peaks in about 0.4 ms at which time the TEV voltage has reached about 85% of

its final value. Thus, the I(V) curve derived from TEV data is likely to be artifactually left-shifted, since peak currents will be measured at times prior to total clamp settling and at voltages more negative than V_{test}. We have previously demonstrated that the I(V) relationship for the slow mode is right-shifted relative to the fast mode (Ruben et al., 1993; Fleig et al., 1994b; Rayner et al., 1994). If, on one hand, the I(V) curve is biased toward hyperpolarized voltages by measuring peak current at a voltage lower than expected, and, on the other hand, biased toward depolarized voltages by selection for the slow mode, these conflicting factors would confound any interpretation of sodium channel voltage-dependence arising from TEV data. In channels where activation and inactivation rates are substantially slower than clamp rise time, these factors become less offensive. Additionally, the artifactual selection for slow-mode channels by slow clamp rise time in TEV can be at least partially reduced through the use of low resistance agarose cushion electrodes (Schreibmayer et al., 1994) which permit faster rise-times.

In addition to our own work with RBIIa channels (Fleig et al., 1994a,b), modal behavior in sodium channels has been previously noted in rat brain and cardiac sodium channels expressed in *Xenopus* oocytes (Moorman et al., 1990; Zhou et al., 1991) and in sodium channels in a variety of other preparations (Patlak and Ortiz, 1985, 1986; Kirsch and Brown, 1989). Developmental appearance of modal gating has also been noted in rat neocortical neurons (Huguenard et al., 1988). Thus, there is ample evidence to support the presence of kinetically different sodium channel gating properties within a single channel population. However, none of the previous studies have elucidated a mechanism for mode selection. Although spontaneous shifts in mode
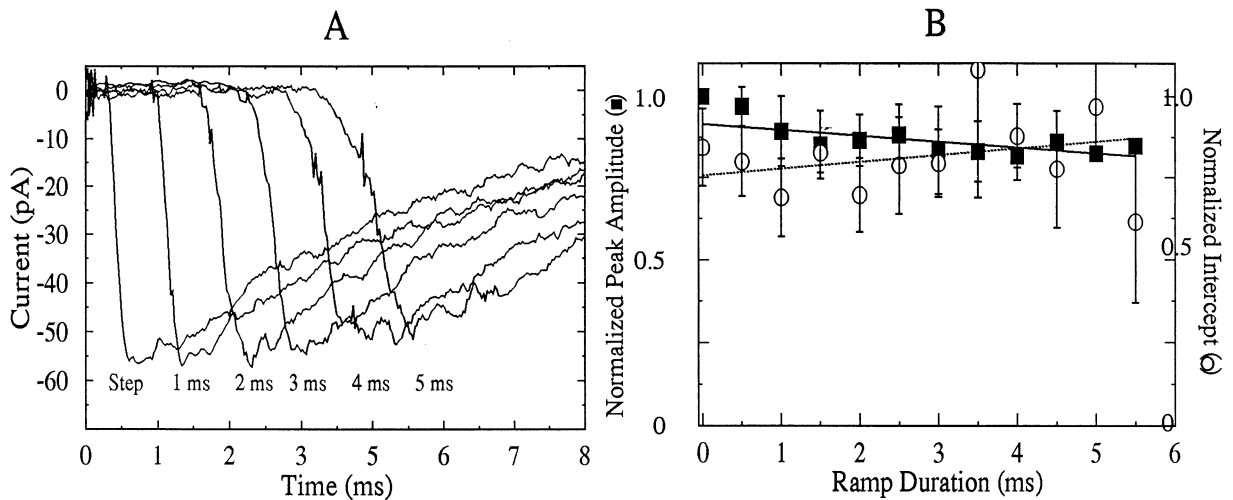
Fig. 4. Slow mode patches are not significantly affected by ramp depolarizations. (A) Shows macroscopic sodium currents recorded during step and ramp depolarizations (ramp durations indicated below each peak current). (B) Graphs peak current amplitudes, normalized to the maximum for each record (solid boxes) and intercepts for test pulse inactivation (open boxes). Currents were best fit by a single exponential. Data shown are means ($\pm$ S.D.; $N = 14$ patches). $V_{pre} = -120$ mV. $V_{test} = 0$ mV.

have been widely observed, the present report is the first (of which we are aware) to describe a method by which gating modes can be experimentally selected using kinetic-sensitivity rather than voltage-sensitivity (Fleig et al., 1994a). Hence, sodium channels may display slower gating kinetics by slowing the rate of voltage change during depolarization, thereby inactivating the fastest gating kinetics.

We can imagine different mechanisms that might account for the sodium channel properties reported here. Several phenomenological kinetic models have been presented that have pathways into the inactivated state from pre-open states (e.g. Armstrong and Bezanilla, 1977; Bezanilla and Armstrong, 1977; Gilly and
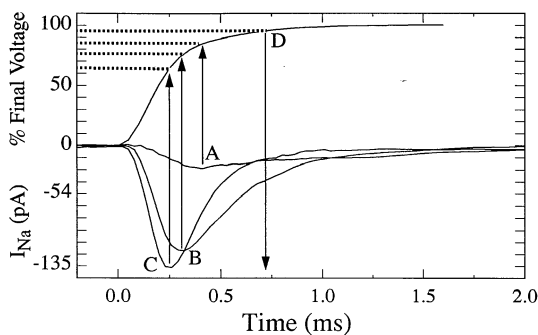

Fig. 5. Macropatch currents compared to TEV clamp rise time. The capacity current from an 80 mV TEV voltage step was integrated to derive clamp rise time (see Alicata et al., 1989). This is shown by the upper trace and corresponds to the ordinate labeled '% Final Voltage'. Currents labeled A, B and C were elicited by voltage steps from V_{hold} -100 mV to V_{test} -40, -20 and 0 mV, respectively, and recorded from an excised macropatch. Dashed lines show percentage of final TEV voltage at which the corresponding macroscopic currents were recorded. D corresponds to the point at which voltage reaches 95% of the final command potential.

Armstrong, 1982; Chahine et al., 1994). Therefore, given an appropriate distribution of relative rate constants, it is also conceivable that fast-mode channels have a greater propensity to inactivate prior to opening. However, the number of channels following this pathway seems to comprise a relatively small fraction of the total population (Aldrich et al., 1983; Goldman, 1989). Thus, it seems unlikely that inactivation from pre-open states during ramp depolarization could account for the loss of what otherwise is a large proportion of open channels. On the other hand, we have recently presented evidence that modes are pharmacologically separable (Starkus et al., 1993). Fast-mode channels might activate and inactivate prior to the peak of the sodium current as membrane voltage first transits through the fast-mode g(V) curve during slow depolarizations. As we discuss below, this mechanism can only account for a small fraction of the peak current suppression we observed with slow ramp depolarizations. Finally, the most credible possibility is that fast-mode channels simply inactivate too rapidly to constitute a significant fraction of the falling phase of macroscopic current recorded during slow ramp depolarizations. This mechanism was more fully explored using simulations (see Section 5).

The physiological implications of different inactivation rates have been previously noted in terms of regulating the rate of repetitive firing (Hotson and Prince, 1980; Stafstrom et al., 1985). Slowly inactivating currents were demonstrated to have less sensitivity to steady-state inactivation and faster recovery from inactivation (Huguenard et al., 1988). The present study reveals one mechanism by which synaptic mechanisms could control firing rates. Thus, slow synaptic depolar-

Table 3
Simulation parameters

Mode	A (μs^{-1})	z	d	$V_{0.5}$ (mV)
Fast				
$C_1 - C_2$	0.0045	0.8	0.5	−48
$C_2 - C_3$	0.0015	1.8	0.5	−48
$C_3 - O$	0.0270	0.8	0.5	−48
$O - I_f$	0.0051	0.2	0.2	−482
Slow				
$C_1 - C_2$	0.0045	0.8	0.5	−38
$C_2 - C_3$	0.0015	1.8	0.5	−38
$C_3 - O$	0.0050	0.8	0.5	−38
$O - I_s$	0.0001	0.2	0.2	−482

izations could select for the slow mode of sodium channel gating resulting in a single action potential during a sustained depolarization. Further studies using single channel analysis will reveal whether the slow mode is due to channel reopenings as in neuroblastoma cells (Aldrich et al., 1983) and oocytes (Krafte et al., 1990) or because of an increase in first-latency or mean open time (Moorman et al., 1990; Zhou et al., 1991).

5. Simulations

Simulations were carried out (see Section 2) to assess the possibility that the faster inactivation rate seen in macropatch experiments would be sufficient to account for selective loss of this kinetic during slow ramp depolarizations. We presumed: first, that this kinetic represents the primary inactivation rate for a separate subpopulation of fast mode channels; second, that the lifetime of each mode is long relative to the 20 ms duration of our test pulses (cf. Zhou et al., 1991). The simplest schema (Eq. (1)) for this simulation is thus the summation of two parallel modes, where each mode is represented as a simple linear model:

$C_1 - C_2 - C_3 - O - I_f$ Fast mode
$C_1 - C_2 - C_3 - O - I_s$ Slow mode

In our simulations the activation parameters were identical for each mode (except that the midpoint for all activation transitions was shifted to the right by 10 mV and the C_3-O reaction was slowed for the slow mode component). However, the 0-I transitions were adjusted to give falling phase eigenvalues of ∼ 0.5 and ∼ 5 ms for the fast and slow modes, respectively (see Table 3 for rate parameters used in these simulations).

Within this system, initial state occupancies at holding potential were obtained by simulating a 500 ms pulse to holding potential (here − 100 mV). Control macropatch kinetics were simulated presuming a 0.1 ms exponential clamp settling time to reach 0 mV test potential. Macropatch ramp depolarizations were simu-

lated as linear ramps with durations of 1, 2, 3, 4 and 5 ms from holding potential to 0 mV test potential.

Fig. 6A shows the results obtained for the full model containing both slow and fast modes (in the ratio 7.5%: 92.5%). Note the selective loss of the fast mode at longer ramp durations. These simulations show a quantitatively similar suppression of peak current and change in the ratio 'time to peak/ramp duration' as the data of Fig. 2A and B. Fig. 6B shows the a simulation of the same model for the ratio 75% slow to 25% fast mode, scaled to the same peak as the combined simulation of Panel A. Note the relative lack of ramp sensitivity when the more slowly inactivating mode predominates. The apparently greater weighting of the slow mode channels in these simulations arises from their longer mean open time and hence greater peak open probability; although this is an interesting finding, it is not necessarily predicted that the same effect would occur in experimental data. Nevertheless these simulations seem fully consistent with our present results.

We recognize that ramp depolarizations, as compared to the slow exponential rise of voltage in TEV, might exacerbate or reduce effects on peak suppression, time to peak and mode selection. To explore the relative effects of linear versus exponential changes in voltage, we repeated the simulations for 1 and 2 ms ramps using exponential changes in voltage with 1 and 2 ms times to final test potential. Exponential rise times were simulated as the sum of two exponential components, such that calculated dv/dt approximated the waveform of experimental capacity current traces.

Whereas a 1-ms ramp suppressed peak current by 18%, an exponential waveform with 1 ms to test potential suppressed peak current by 20%. Time to peak in a 1 ms ramp is 4-fold longer than in the control, and only 2.4-fold longer using a 1 ms exponential voltage change. For a 2-ms ramp, the peak current was suppressed by 45% as compared to 36% for a 2-ms exponential voltage change. Time to peak was 7-fold longer than control for a 2-ms ramp, and only 3.6-fold slower using a 2-ms exponential voltage waveform. There was no significant difference in the relative proportions of fast versus slow mode between the ramp and exponential simulations. Thus, we conclude that although the ramp depolarizations slightly exaggerate the time-domain effects of slow clamp rise-time when compared to exponential waveforms, the effect on the I(V) relationship is approximately the same. Hence, both slow ramps and slow exponentials distort the midpoint of activation. Ramp depolarizations provide a simple method for preliminary studies on the effects of slow clamp rise-times.

Additional simulations (not shown) were carried out to assess the relative importance of the I(V) shift versus the change in inactivation rate. Suppression at 5 ms increased from 8% (as in Fig. 6B) to 15% when the
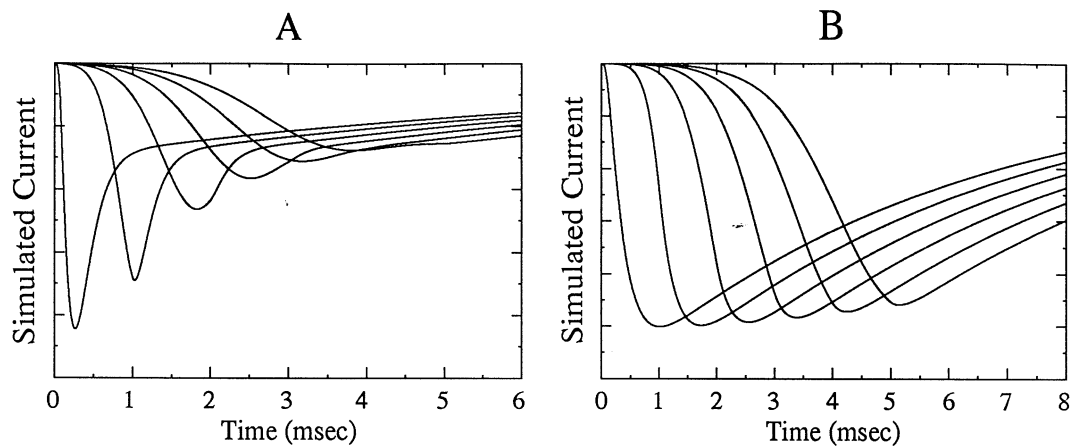
Fig. 6. Simulations of ramp sensitivity. See text for explanation. Compare A to Fig. 2A. Compare B to Fig. 4A.

midpoints were the same for both fast and slow modes (as compared to a 66% suppression in Fig. 6A). Thus the suppression of fast mode channels by ramp depolarizations clearly derives primarily from the difference in inactivation rate between these modes.

Acknowledgements

References

Alicata, D.A., Rayner, M.D. and Starkus, J.G. (1989) Osmotic and pharmacological effects of formamide on capacity current, gating current and sodium current in crayfish giant axons. Biophys. J., 55: 347–353.

Aldrich, R.W., Corey, D.P. and Stevens, C.S. (1983) A reinterpretation of mammalian sodium channel gating based on single channel recording, Nature, 306: 436–441.

Armstrong, C.M. and Bezanilla, F. (1977) Inactivation of the sodium channel. II. Gating current experiments, J. Gen. Physiol., 70: 567–590.

Auld, V.J., Goldin, A.L., Krafte, D.S., Marshall, J., Dunn, J.M., Catterall, W.A., Lester, H.A., Davidson, N., and Dunn, R.J. (1988) A rat brain Na$^+$ channel α-subunit with novel gating properties, Neuron, 1: 449–461.

Bezanilla, F. and Armstrong, C.M. (1977) Inactivation of the sodium channel. I. Sodium current experiments, J. Gen. Physiol., 70: 549–566.

Chahine, M., George, A.L., Zhou, M., Ji, S., Sun, W., Barchi, R.L., and Horn, R. (1994) Sodium channel mutations in paramyotonia congenita uncouple inactivation from activation, Neuron, 12: 218–294.

Chiu, S.Y. (1977) Inactivation of sodium channels: second order kinetics in myelinated nerve, J. Physiol., 273: 573–596.

Cummins, T.R., Zhou, J., Sigworth, F.J., Ukomadu, C., Stephan, M., Ptacek, L.J. and Agnew, W.S. (1993) Functional consequences of a Na$^+$ channel mutation causing hyperkalemic periodic paralysis, Neuron, 10: 667–678.

Cummins, T.R., Xia, Y. and Haddad, G.G. 1994. Functional properties of rate and human neocortical voltage-sensitive sodium currents, J. Neurophysiol., 71: 1052–1064.

Fleig, A., Ruben, P.C. and Rayner, M.D. (1994a) Kinetic mode switch of rat brain IIA sodium channels in *Xenopus* oocytes excised macropatches, Pfluger's Arch., 427: 399–405.

Fleig, A., Fitch, J.M., Goldin, A.L., Rayner, M.D., Starkus, J.G. and Ruben, P.C. (1994b) Point mutations in IIS4 alter activation and inactivation of rat brain IIA sodium channels in *Xenopus* oocyte macropatches, Pfluger's Arch., 427: 406–413.

Gilly, W. and Armstrong, C.M. (1982) Slowing of sodium channel opening kinetics in squid axon by extracellular zinc, J. Gen. Physiol., 79: 935–964.

Goldman, L. (1989) Sodium channel opening as a precursor to inactivation: a route to the inactivated state, Eur. Biophys. J., 16: 321–325.

Goldin, A.L., Snutch, T., Lubbert, H., Dowsett, A., Marshall, J., Auld, V., Downey, W., Fritz, L.C., Lester, H.A., Dunn, R., Catterall, W.A. and Davidson, N. (1986) Messenger RNA coding for only the a subunit of the rat brain Na channel is sufficient for expression of functional channels in Xenopus oocytes. Proc. Natl. Acad. Sci. USA, 83: 7503–7507.

Hille, B. (1992) Ionic Channels of Excitable Membranes, 2nd Edn, Sinauer, Sunderland, MA, USA, pp. 24.

Hodgkin, A.L. and Huxley, A.F. (1952) A quantitative description of membrane current and its application to conduction and excitation in nerve, J. Physiol. London, 117: 500–544.

Hotson, J.R. and Prince, D.A. (1980) A calcium-activated hyperpolarization follows repetitive firing in hippocampal neurons, J. Neurophysiol., 43: 409–419.

Huguenard, J.R., Hamill, O.P. and Prince, D.A. (1988) Developmental changes in Na conductances in rat neocortical neurons: appearance of a slowly inactivation component, J. Neurophysiol., 59: 778–795.

Isom, L.L., deJongh, K.S., Patton, D.E., Reber, B.F., Offord, J., Charbonneau, H., Walsh, K., Goldin, A.L. and Catterall, W.A. (1992) Primary structure and functional expression of the beta 1 subunit of the rat brain sodium channel, Science, 256: 839–842.

Kass, R.S., Sieglebaum, S.A. and Tsien, R.W. 1979. Three micro-electrode voltage clamp experiments in calf cardiac purkinje fibres: is slow inward current adequately measured? J. Physiol., 290: 201–225.

Kirsch, G.E. and Brown, A.M. (1989) Kinetic properties of single sodium channels in rat heart and rat brain, J. Gen. Physiol., 93: 85–99.

Krafte, D.S., Goldin, A.L., Auld, V.J., Dunn, R.J., Davidson, N. and Lester, H.A. (1990) Inactivation of cloned Na channels expressed in *Xenopus* oocytes, J. Gen. Physiol., 96: 689–706.

Li, M., West, J.W., Lai, Y., Scheuer, T., and Catterall, W.A. (1992) Functional modulation of brain sodium channels by cAMP-dependent phosphorylation, Neuron, 8: 1151–1159.

Lux, H.D. and Pollen, D.A. (1966) Electrical constants of neurons in the motor cortex of the cat, J. Neurophysiol., 29: 207–220.

McClatchey, A.I., Cannon, S.C., Slaugenhaupt, S.A. and Gusella, J.F. (1993) The cloning and expression of a sodium channel beta 1 subunit cDNA from human brain, Hum. Mol. Genet., 2: 745–749.

McCormick, D.A., Conners, B.W., Lighthall, J.W. and Prince, D.A. (1985) Comparative electrophysiology of pyramidal and sparsely spiny stellate neurons of the neocortex, J. Neurophysiol., 54: 782–805.

Moorman, J.R., Kirsch, G.E., Brown, A.M., and Joho, R.H. (1990) Changes in sodium channel gating produced by point mutations in a cytoplasmic linker, Science, 250: 688–691.

Patlak, J.B. and Ortiz, M. (1985) Slow currents through single sodium channels of the adult rat heart, J. Gen. Physiol., 86: 89–104.

Patlak, J.B. and Ortiz, M. (1986) Two modes of gating during late Na channel currents in from sartorius muscle, J. Gen. Physiol., 87: 305–326.

Patton, D.E., West, J.E., Catterall, W.A. and Goldin, A.L. (1992) Amino acid residues required for fast Na$^+$-channel inactivation: charge neutralizations and deletions in the III-IV linker, Proc. Natl. Acad. Sci. USA, 89: 10905–10909.

Rayner, M.D., Featherstone, D., Andres, M., Lu, J., Henteleff, M., Ruben, P.C. and Starkus, J.G. (1994) Evaluating sodium channel mutants: macroscopic correlates of mode changes, Biophys. J., 66: A102.

Ruben, P.C., Fleig, A., Rayner, M.D. and Starkus, J.G. (1993) Sodium channel IIa: changes in sensitivity to dv/dt following single point mutations in IIS4, Biophys. J., 64: A87.

Scheuer, T., Auld, V.J., Boyd, S., Offord, J., Dunn, R. and. Catterall, W.A. (1990) Functional properties of rat brain sodium channels expressed in a somatic cell line, Science, 247: 854–858.

Schreibmayer, W., Lester, H.A. and Dascal, N. (1994) Voltage clamping of *Xenopus laevis* oocytes utilizing agarose cushion electrodes, Pfluger's Arch., 426:4 53–458.

Starkus, J.G., Rayner, M.D., Fleig, A. and Ruben, P.C. (1993) Fast and slow inactivation of sodium channels: effects of photodynamic modification by methylene blue, Biophys. J., 65: 715–726.

Stafstrom, C.E., Schwindt, P.C., Chubb, M.C. and Crill, W.E. (1985) Properties of persistent sodium conductance and calcium conductance of layer V neurons from cat sensorimotor cortex in vitro, J. Neurophysiol., 53: 153–170.

Stühmer, W., Conti, F., Suzuki, H., Wang, X., Noda, M, Yahagi, N., Kubo H. and Numa, S. (1989) Structural parts involved in activation and inactivation of the sodium channel, Nature, 339: 597–603.

Ukomadu, C., Zhou, J., Sigworth, F.J. and Agnew, W.S. (1992) μ1 Na$^+$ channels expressed transiently in human embryonic kidney cells: biochemical and biophysical properties, Neuron, 8: 663–676.

West, J.W., Patton, D.E., Scheuer, T., Wang, Y., Goldin, A.L. and Catterall, W.A. (1992) A cluster of hydrophobic amino acid residues required for fast Na$^+$-channel inactivation, Proc. Natl. Acad. Sci. USA, 89: 10909–10914.

Yang, J.S., Bennett, P.B., Makita, N., George, A.L. and Barchi, R.L. (1993) Expression of the sodium channel beta 1 subunit in rat skeletal muscle is selectively associated with the tetrodotoxin-sensitive alpha subunit isoform, Neuron, 11: 915–922.

Zhou, J., Potts, J.F., Trimmer, J.S., Agnew, W.S. and Sigworth, F.J. (1991) Multiple gating modes and the effect of modulating factors on the μ1 sodium channel, Neuron 7: 775–785.